Nucleation delay in water-saturated rhyolite during decompression in shallow volcanic systems and its implications for ascent dynamics

Monika K. Rusiecka, Caroline Martel

Nucleation delay in water-saturated rhyolite during decompression in shallow volcanic systems and its implications for ascent dynamics

Monika K. Rusiecka[1, *]

Caroline Martel[1]

[1]**Institut des Sciences de la Terre d'Orléans, Université d'Orléans-CNRS-BRGM UMR 7327, F-45071 Orléans, France**

[*]**monika.k.rusiecka@gmail.com (corresponding author)**

Abstract

We developed a model of feldspar nucleation delay during decompression in water-saturated rhyolite based on classical nucleation theory (CNT). With the thermodynamic and kinetic parameters proposed in this study, the model agrees with the experimental results of this study to within a factor of two. To account for the variety of conditions encountered by magma during ascent, we propose expanding the model, developed in this study for isothermal decompression, to a wider range of pressures and temperatures (i.e., non-isothermal conditions). We present new measurements of feldspar growth rates during decompression in water-saturated rhyolite, emphasizing the importance of accurately calculating the nucleation delay in order to estimate growth rates. Using these data, we propose a method for estimating the ascent rate of water-saturated rhyolite based on the nucleation delay of feldspar microlites. The findings of this study hold the promise of a better understanding of volcanic timescales during magma ascent in the conduit, as well as the possibility of extending our model to more complicated scenarios with changing pressure and temperature.

Keywords:

nucleation delay, ascent rate, crystallization, decompression, magmatic timescales

Introduction

Microlites, the crystals less than few hundred micrometers in size, of which plagioclase is the most common, form on the timescales of minutes to a few days during magma ascent and subsequent degassing (e.g., Sharp et al. 1996, Hammer et al. 1999, Hammer and Rutherford 2002, Martel 2012, Mollard et al. 2012). Because they form on the timescales of ascent their presence and textures can provide valuable information about magma ascent rates and conditions in the conduit. Moreover, timing of crystallization can affect the production of crystal-rich or crystal-poor magmas, resulting in changes in the textural make-up of the produced rock as well as the explosivity. Magma composition and exsolution of dissolved volatiles are the primary determinants of eruption style and timing. The presence of crystals, on the other hand, can impact volatile exsolution by acting as nucleation sites for bubble nucleation (e.g., Hurwitz and Navon 1994, Gardner and Denis 2004, Shea 2017, Pleše et al. 2018) and magma rheology (D'Oriano et al. 2005, Mader et al. 2013, Vona et al. 2017). The permeability of vesicular magma can be affected by crystallization during ascent, which can lead to changes in eruption style by lowering the percolation threshold and changing the eruptive behaviour from explosive to effusive (e.g., Lindoo et al. 2016, Cassidy et al. 2018, deGraffenried et al. 2019). Notably, magmas with ~4.0-5.5 wt. % water (around the water saturation limit depending on storage conditions) and <30 vol. % crystallinity erupt mostly explosively, but magmas with >40 vol. % crystallinity erupt primarily effusively (Popa et al. 2021).

The first order transition i.e., nucleation initiates the process of partial or complete crystallization of a silicate melt (e.g., Kirkpatrick 1981, De Yoreo and Vekilov 2004, Fokin et al. 2006). Nucleation is the process of rearrangement of atoms (or molecules) in a parent phase that results in the formation of a cluster of a new, thermodynamically more stable phase (Kirkpatrick 1981, De Yoreo and Vekilov 2004, Fokin et al. 2006). In magmatic systems, however, nucleation does not occur immediately when the new phase becomes thermodynamically stable, istead can be delayed by minutes, hours, or days (e.g., Fenn 1977, Swanson 1977, Couch 2003, Mollard et al. 2012, Polacci et al. 2018, Rusiecka et al. 2020). Understanding the magmatic timescales of volcanic systems can be improved by studying nucleation kinetics, particularly nucleation delay. Modelling nucleation delay allows for the prediction of the

timescales on which igneous rocks crystallize from a melt and when they do remain vitreous (Rusiecka et al. 2020). Numerous studies have been conducted to investigate crystallization kinetics in felsic melts (e.g., Fenn 1977, Swanson 1977, Hammer and Rutherford 2002, Couch 2003, Brugger and Hammer 2010, Mollard et al. 2012, Riker et al. 2015, Sirbescu et al. 2017, Mollard et al. 2020, Rusiecka et al. 2020). However, the majority of these studies have been focused on constraining the crystal growth and nucleation rates. A few of them provided incidental measurements of nucleation delays (e.g., Fenn 1977, Swanson 1977, Couch 2003, Mollard et al. 2012, Sirbescu et al. 2017). Rusiecka et al. (2020) presented a model based on Classical Nucleation Theory (CNT) for the nucleation delay of plagioclase, pyroxene and olivine in basaltic melts, and of quartz and alkali feldspar in a hydrous, rhyolitic melt under isobaric conditions.

In this contribution we build on the model presented by Rusiecka et al. (2020) by developing a theoretical model of feldspar nucleation delays in rhyolitic melts during ascent in the conduit. The model was calibrated by a series of decompression-induced crystallization experiments conducted using a hydrated obsidian at temperatures ranging from 800-900 °C and pressures ranging from 25-200 MPa. This temperature range is representative of natural rhyolite temperatures (e.g., Castro and Dingwell 2009) and decompression from 200 to 25 MPa covers the range of pressures prevailing during magma ascent from a deep reservoir (200 MPa, around 7.5 km below the Eart's surface) to near-surface levels (Martel, 2012).

Classical Nucleation Theory

Volmer and Weber (1926), Becker and Döring (1935), and Turnbull and Fisher (1949) developed classical nucleation theory during the first half of the twentieth century on the basis of Gibbs' (1875-1878) earlier work on the thermodynamic description of heterogeneous systems. According to Gibbs' theory, a heterogeneous system, consisting of a parent phase and a new nucleating phase, is replaced for simplicity, by two homogeneous phases (the parent and a nucleus) divided by a mathematical surface of zero thickness. A change in Gibbs free energy between the newly formed nucleus and the parent phase drives nucleation. The parent phase is assumed to be in a metastable state, and nucleation must occur after an

activation energy barrier is overcome. The rate of nucleation is affected by the degree of supersaturation, which is commonly measured as undercooling below the liquidus temperature. When the new nuclei are surrounded by the previously existing phase, homogeneous nucleation occurs, and heterogeneous nucleation occurs when the nucleating phase forms on a previously existing surface (Kirkpatrick 1981, De Yoreo and Vekilov 2004, Fokin et al. 2006).

Methods

Experimental procedure

The starting sample used in the experiments is the Lake County Obsidian (LCO) – a common metaluminous composition (in wt. % on an anhydrous basis: 75.7 SiO_2, 0.1 TiO_2, 13.2 Al_2O_3, 0.7 FeO, 0.1 MnO, 0.1 MgO, 0.6 CaO, 4.3 Na_2O, 5.1 K_2O; Maneta and Baker 2014). This is the same material as used to investigate cooling-induced crystallization by Rusiecka et al. (2020) and Rusiecka and Baker (2021). The obsidian was coarsely crushed and melted at 1400 °C for 4 hours before being ground to a fine powder. About 30 mg of the LCO glass powder was loaded into 15 mm length 2.9 mm OD (outer diameter), 2.5 mm ID (inner diameter) gold capsules with enough water to ensure saturation (as calculated using MagmaSat, Ghiorso and Gualda 2015) and welded shut. To check for leaks, the capsules were kept at 120 °C for at least 2 hours and weighed. The experiments were carried out at the Institut des Sciences de la Terre d'Orleans in Orleans (France) in an Internally Heated Pressure Vessel (IHPV) with argon as the pressurizing medium. The capsules were placed in the 3-cm hot spot of the furnace and temperature (±4 °C) was controlled at the top and bottom of the samples using two S-type thermocouples. The pressure (±2.5 MPa) was monitored by a high pressure transducer calibrated against a 700 MPa Heise gauge. The liquidus temperature at different pressures was determined using rhyolite-MELTS (Ghiorso and Sack 1995, Gualda et al. 2012) and confirmed experimentally at 200, 150 and 50 MPa to constrain the effective degree of undercooling (ΔT_{eff} = run temperature – liquidus temperature, Table 1). To confirm that the starting material was free of pre-existing crystals we conducted an experiment in which the samples were kept for 24 h at 825 °C and 200 MPa and then decompressed at 10 MPa/min to

50 MPa. They were then immediately isobarically quenched. Experiments were first kept at 200 MPa and 825 °C for 24 hours to homogenize the melt with water and then decompressed at 10 MPa/min to 90, 75, 50 and 25 MPa (Table 1).

Analytical techniques

After the experiments, the capsules were first weighted to confirm that no water loss occurred during the experiment. Then they were opened, and the samples were recovered as glass chips that were placed in epoxy resin and polished for analyses. The samples were imaged using a Merlin Compact Zeiss scanning electron microscope (SEM) at the Institut des Sciences de la Terre d'Orléans in Orléans. Although most of the crystals were too small for thorough quantitative analysis the observed crystals were identified as plagioclase feldspar (i.e., in the oligoclase field in the experiment conducted at 50 MPa; semi-quantitative composition: $An_{28}Ab_{65}Or_7$) and magnetite using a Bruker Quantax XFlash6 energy dispersive spectrometer coupled to the SEM. The crystallinity of the samples did not exceed ~1-2 vol. %. The water saturation content was calculated using the MagmaSat application, which employs the Ghiorso and Gualda (2015) H_2O-CO_2 saturation model.

Theoretical model

Nucleation delay (τ) is the time between when the parent phase (silicate melt) is cooled below its liquidus temperature and the onset of crystallization. It is defined as:

$$\tau = \frac{16h}{\pi} \frac{\sigma}{\Delta G_v^2 a^4} exp \frac{E_a}{RT} \quad (1)$$

where h is Planck's constant, R is the gas constant, σ is the interfacial free energy between the parent phase and the forming nucleus. The value for the interfacial free energy was chosen to be 0.18 J/m^2, this being the value of the interfacial free energy for silicate crystals in the system Na_2O-CaO-SiO_2 (Fokin et al. 2006). The interfacial free energy, this being σ, is poorly constrained and for feldspar in a silicate melt can vary between 0.10 and 0.25 J/m^2 (e.g., Hammer 2004, Baker et al. 2020, Mollard et al. 2020, Rusiecka et al. 2020). Free energy of crystallization per unit volume ΔG_V (Robie and Bethke 1962) was calculated

using the MELTS software (Ghiorso and Sack 1995, Gualda et al. 2012). Energy of crystallization, ΔG was obtained using the affinities of feldspar in the melt of the same composition as the starting material at the temperature of the experiments (825 °C) and a range of pressures (10 to 200 MPa). The affinities were plotted against pressure and fitted with a trend line. The equation describing the trend line was used in the calculation of the ΔG in the nucleation delay program. Parameter a in Equation (1) is the size of a structural unit, here approximated using the size of the Si^{4+} ion (0.26×10^{-10} m, Shannon 1976), as Si^{4+} is an essential component of both a silicate melt and its crystals. This value was previously successfully used by Rusiecka et al. (2020) for nucleation of quartz and feldspar in a natural, hydrous rhyolite, and by Baker et al. (2020) for anorthite and diopside in a synthetic composition. The activation energy for nucleation (E_a, the kinetic barrier) was approximated using the diffusivity calculated using the Eyring equation (Eyring 1935):

$$E_a = -k_B T ln\left(\frac{h}{\lambda^3 \eta}\right) \quad (2)$$

where η is viscosity and λ is the size of the diffusive jump and k_B is the Boltzmann's constant. The diffusive jump is not well constrained and can generally vary between 1^{-10} to 5^{-10} m (0.1 to 0.5 nm, e.g., Baker 1990, 1992, Mungall 2002, Gonzalez-Garcia et al. 2017). The variation of the diffusive jump from 1^{-10} m to 5^{-10} m corresponds to variation in a nucleation delay of two orders of magnitude. The viscosity for the Eyring equation was calculated using model by Giordano (2008) with water contents calculated at saturation at the different run pressures using the MagmaSat program (i.e., 1.8 to 4.8 wt. % H_2O from 25 to 120 MPa). Rusiecka et al. (2020) proposed that activation energy for the nucleation needs to be modified by using diffuse interface theory. However, this is not the case in this study as using the parameters for water saturated melt and changing the water content at saturation with pressure replicates the experimental results to within a factor of two. This variation might be caused by the differences in water content and the distribution of water in the melt. In the case of Rusiecka et al. (2020) water content

was 4 wt. %, which is several wt. % below the saturation content at the experimental conditions (600 MPa) whereas in this study all the experiments were water saturated.

The numerical constant in Equation 1 ($\frac{16}{\pi}$) is that of Fokin et al. (2006); different derivations of Equation (1) (e.g., Collins 1955, Kashchiev 1969, Slezov and Schmelzer 1999, 2002) can lead to slightly different constant values, but they typically vary by less than an order of magnitude (Gutzow and Schmelzer 1995).

Results

Description of the textural characteristics of the experimentally produced plagioclase

All samples produced in experiments conducted in this study are vesicular and contain magnetite. Although magnetite may be seen as inclusion in some feldspars on the SEM images, it is not considered here as a nucleation site for the silicate crystals for two main reasons. Firstly, the distribution of the oxides in connection to the plagioclase is random (i.e., there are more oxide sites than plagioclase crystals). Secondly, the magnetite distribution within the plagioclase crystals is random (i.e., magnetite is not systematically in the centre of the plagioclase where growth would presumably have started in case of magnetite acting as a preferential nucleation site). The sub-micron oxides were likely included in the plagioclase during rapid growth. Plagioclase was produced at three different pressures: 90, 75 and 50 MPa (corresponding to ΔT_{eff} = -10, -20 and -55 °C). The representative images of the samples produced at those conditions can be observed in Figure 1. Magnetite and plagioclase crystals are homogeneously distributed in the sample and did not preferentially nucleated at capsule walls. At 50 MPa (ΔT_{eff} = -55 °C) the crystals are highly irregular with skeletal morphologies (Fig. 1a) and numerous embayments and melt inclusions (Fig. 1b). At 75 MPa (ΔT_{eff} = -20 °C) the crystals are more regular than at 50 MPa and have more prismatic shapes, nevertheless some irregularities, melt embayments and inclusions persist (Fig. 1c). At 90 MPa (ΔT_{eff} = -10 °C) the crystals are elongated, with euhedral and subhedral morphologies, well faceted crystals (Fig. 1d), and some clustering of smaller crystals.

Nucleation delay

171 The theoretically derived curve describing nucleation delay of plagioclase in hydrous, metaluminous
172 rhyolite at the conditions of the experiments in this study is shown in Figure 2 along with the experimental
173 results. In our study, the shortest delay is 30 h at ΔT_{eff} -50 °C, and the delay tends to infinity as the
174 undercooling approaches zero. The findings of our study, as well as our modeling of the nucleation delay
175 in decompression induced crystallization, were compared to those of Mollard et al. (2012), who
176 conducted experiments on a rhyolitic melt using a crystal free starting material and reported nucleation
177 delays in their study (nucleation delays are given in Fig. 7 of Mollard et al. 2012). We initialized
178 nucleation delay model with a value for interfacial free energy of 0.18 J/m^2, and bracketed it with values
179 ranging from 0.10 J/m^2 to 0.25 J/m^2. Our theoretical modelling is specific to the composition used in this
180 study, but agrees well with other rhyolitic compositions represented by the synthetic composition of
181 Mollard et al. (2012), as shown here in Figure 2. Considering both the experiments conducted in this
182 study as well as the experiments of Mollard et al. (2012), the model agrees with the experimental data
183 by a factor of two, which is also the uncertainty represented by the typical variation in range of the
184 interfacial free energy.

185 **Growth rates**

186 We calculated the growth rates of feldspar (G_{max}) in the samples where crystallization was observed. To
187 do this we used ten largest crystals from each sample and applied growth rate equation (e.g., Couch 2003,
188 Arzilli and Carroll 2013, Arzilli et al. 2020, Rusiecka and Baker 2021) modified to include nucleation
189 delay:

190 $$G_{max} = \frac{(L/2)}{(t-\tau)} \quad (3)$$

191 Here, L is the length of the longest crystal dimension (in m), t is the duration of the experiment (in s) and
192 τ is the nucleation delay calculated using the model described above. The spreadsheet with all the growth
193 rates obtained is available in the Supplementary Material.

Growth rates for pressures of 90, 75 and 50 MPa (corresponding to ΔT_{eff} = -10, -20 and -55 °C) are shown in Figure 3. At the conditions of these experiments (i.e., moderate to low degrees of undercooling) the growth rates are on the order of 10^{-11} m/s (10^{-8} mm/s), and increases from the lowest degree of undercooling to the highest degree of undercooling.

When plotting the growth rates for experiments conducted at 50 MPa (ΔT_{eff} = -55 °C) with different durations (48, 72 and 120 h, Fig. 4), higher by about a factor of two in the first, shor experiment than in the subsequent, longer experiment. Growth rates decrease with time is not unexpected. We expect non-linear behaviour due to the rapid decay of initial steep gradients in chemical potential (c.f., Moschini et al. 2021). The decay in the growth rates can be best represented semi-quantitatively by fitting the experimental results with a trend line, as in Figure 4.

Another way of looking at growth rates is by comparing them to the equilibrium growth rate (G) as calculated using the dependence of growth rate on the degree of undercooling (Equation 4; Toramaru 1991, Moschini et al. 2021):

$$G \propto exp\left(\frac{-E_a}{RT_{exp}}\right)\left(1 - exp\frac{\Delta H \Delta T}{RT_{exp}T_L}\right) \quad (4)$$

Here, E_a is the activation energy (approximated as the activation energy of diffusion from Eq. 2 with the same parameters as in the nucleation delay calculation), T_{exp} is the temperature at which the experiment was conducted, ΔH is enthalpy of fusion (extracted from MELTS), and T_L is the liquidus temperature. Growth rates calculated using Equation (4) yield results on the same order of magnitude as the growth rates derived from experimental results with nucleation delay taken into account. Moreover, the growth rate at 50 MPa most closely matches the growth rate derived from the longest experiment suggesting that after dissipation of the initial steep chemical potential gradients, the growth rate trends to equilibrium over time. In the case of growth of plagioclase, at 50 MPa the equilibrium growth rate is achieved after ~95 h (120 h of the experimental duration minus ~25 h for the nucleation delay).

Discussion

Using nucleation delay to estimate the ascent rate in microlite-free and microlite-bearing rhyolites

Textures of volcanic products are strongly linked to the history of magma ascent (e.g., Noguchi et al. 2006, Polacci et al. 2006, Bain et al. 2021) . On eruptive timescales, degassing of volatile-rich magma can induce feldspar microlite formation, although this growth can be hindered if the ascent is too fast (c.f., Hammer and Rutherford 2002). For volcanic hazard reduction, estimating the ascent rates during an eruptions is crucial, as it can determine the style of eruption (e.g., Dingwell, D.B. 1996, Castro and Gardner 2008, Mujin and Nakamura 2014). Typical ascent rates derived for rhyolitic eruptions are in the range of 0.00005 to 5 MPa/s, corresponding to ascent velocities of 0.0001 to 200 m/s (Rutherford 2008). Figure 5 presents the comparison between depressurization equivalent ascent rates of 0.0005 MPa/s, 0.001 MPa/s, 0.005 MPa/s and 0.01 MPa/s, and the nucleation delay of feldspar in water saturated rhyolite. The starting pressure for the ascent paths, simulating the initial storage conditions, is 120 MPa. For the composition considered at 825 °C these conditions are above the liquidus. The heterogeneous nature of nucleation requires using the correction factor (τ_{het}):

$$\tau_{het} = \tau\varphi^{\frac{1}{3}} \quad (5)$$

where

$$\varphi = \frac{1}{2} - \frac{3}{4}cos\theta + \frac{1}{4}cos^3\theta \quad (6)$$

here θ is the interior contact angle between the surface upon which nucleation occurs and the nucleating phase (Gutzow and Schmelzer 1995; Fokin et al. 2006). The angle used here (25°) is the median wetting angle for feldspar crystals in rhyolite (Holness 2006). In the case of homogeneous nucleation, none of the ascent paths cross the nucleation delay curve except for the path with an ascent rate of 0.0005 MPa/s. The presence of microlites in a water-saturated rhyolite under conditions considered in this study would mean that if the ascent started at the superliquidus storage conditions of 120 MPa and 825 °C, then the minimum ascent rate would be between 0.0005 and 0.001 MPa/s. If no feldspar microlites were produced, the maximum ascent rate would be 0.001 MPa/s. Presence of pre-

existing crystals in the melt subjected to decompression may influence the nucleation kinetics during ascent by decreasing the interfacial free energy between the parent phase (melt) and new nuclei, consequently decreasing the nucleation delays (c.f., Martel 2012, Rusiecka et al. 2020). In case of heterogeneous nucleation delay (Fig. 5) the ascent path crosses the nucleation delay curve at 0.005 MPa/s and not at 0.01 MPa/s, suggesting that in the absence of microlites or overgrowths on pre-existing crystals the maximum ascent rate was 0.01 MPa/s. If microlites or overgrowths are present the minimum ascent rate declines, for this case, to 0.005 MPa/s. This simple model makes it possible to estimate the maximum ascent rate of the crystal free rhyolite, and the minimum ascent rate of microlite-bearing rhyolite.

An example of how presence or absence of microlites can be used to estimate the ascent rate is the 2008 eruption of Chaitén (Northern Patagonia, Chile). There has been discussion as to the reason of the lack of microlites in the products of this eruption (Andrews and Befus 2020, Huggins et al. 2021). Andrews and Befus (2020), who in presenting their Supersaturation Nucleation and Growth of Plagioclase (SNGPlag) numerical model, suggested that the reason their model was unable to reproduce the crystal poor textures of the 2008 Chaiten eruption was the fact that they did not include nucleation delay in their calculations. Castro and Dingwell (2009) performed decompression experiments to determine the minimum decompression rate which resulted in the textures observed in the products of the 2008 eruption. They observed that decompression at 10 MPa/h and 20 MPa/h (~0.005 MPa/s) produced an overgrowth on pre-existing plagioclase crystals but the rim did not form as a result of decompression at 40 MPa/h (~0.01 MPa/s). This result agrees well with the model presented here, where the nucleation delay curve for heterogeneous nucleation crosses the ascent path at 0.005 MPa/s suggesting formation of plagioclase at this ascent rate, but not at 0.01 MPa/s. This indicates that the ascent of 0.01 MPa/s is too fast for the plagioclase to form.

Modelling nucleation delay in Pressure-Temperature (PT) space

Because just one isothermal decompression scenario is used, the nucleation delay model described above may have limited utility in calculating nucleation delays of feldspar in rhyolitic compositions across a wide range of conditions. However, the successful comparison of the nucleation delay model to the decompression results of this study, and the isobaric tests of Rusiecka et al. (2020), allow for the construction of a model of nucleation delay change with pressure and temperature. The nucleation delay at different pressures and temperatures was calculated using a 40 by 40 grid of P and T with a pressure step of 25 bars (2.5 MPa). This corresponds to the uncertainty of the pressure in the experiments and the temperature step of 5 °C. Figure 6 shows the results of modelling of nucleation delay from 100 MPa to 10 MPa and for temperatures from 800 °C to 650 °C. The highest nucleation delays are observed close to the liquidus, at high pressure and temperature, and at the highest degree of undercooling, at low pressure and temperature. At low pressure and temperature there is a high degree of undercooling and the nucleation delay is primarily controlled by the activation energy. Therefore the barrier preventing nucleation is mainly kinetic. At high pressure and temperature, close to the liquidus, the nucleation is mostly hindered by the thermodynamic barrier, i.e., the interplay between the surface and bulk free energy.

Our findings may expand the use of nucleation delay and crystallization of microlites into more complicated magma ascent scenarios, for example: one in which the temperature is not constant during decompression. Thermodynamic modelling of magma degassing without crystallization indicates that both heating and cooling is possible (c.f., Mastin and Ghiorso 2001, Glazner 2019). Not only can the degassing result in a change in temperature during decompression, but also the latent heat released during crystallization of phases not considered in the nucleation delay model may increase the temperature of the magma (c.f., Couch et al. 2001, Blundy et al. 2006). Such phases include those that may nucleate before plagioclase, such as Fe-Ti oxides, pyroxene, and amphibole. The results from our modelling are available in Supplementary material.

Re-evaluating feldspar growth rates

Growth rates when the nucleation delay is considered are twice to three times faster than when the growth is considered throughout the whole experiment (Fig. 3). The same can be observed when comparing growth rates obtained at 50 MPa and for different durations, with the largest difference being visible when comparing growth rates for the shortest experiments (Fig. 4). Growth rates calculated with and without consideration of the nucleation delay have been fitted with an exponential trend as described in Figure 4. The trend line for growth rates calculated without nucleation delay has the same, but the intercept two times lower.

It is especially important to account for the nucleation delay when the timescales being considered are on the same order of magnitude as the delay. This is the case for our experiments, as well as when considering the formation of microlites in an ascending magma where timescales are short i.e., velocities and decompression rates are fast. Experimental growth rates adjusted for delayed nucleation and applied to volcanic systems, can thus help to constrain the minimum ascent rate based on the presence and size of the microlites. When calculating growth rates we need to, however, not only consider the delayed nucleation, but also the deviation from the equilibrium growth rate.

Growth rates obtained in this study fall within the range of growth rates determined in previous studies on decompression induced crystallization in felsic melts (e.g., Hammer and Rutherford 2002, Couch 2003, Martel 2012, Mollard et al. 2012, Riker et al. 2015). Our growth rates are compared to the results of other experimental studies on silicic melts in which the single step decompression (SSD) method was employed in (Fig. 3).

Mollard et al. (2012) obtained the growth rates one order of magnitude higher than in our study at similar ΔT_{eff} whereas the growth rates in Hammer and Rutherford (2002) and Couch (2003) are of the same order of magnitude as obtained here. One reason for this discrepancy may be the effect of composition. This study and the studies of Hammer and Rutherford (2002) and Couch (2003) used compositions with SiO_2 contents of less than 75 wt. % and containing K_2O. Mollard et al. (2012) used a high silica composition (SiO_2 = 78.7 wt. %) and with no K_2O. The growth rates of Hammer and Rutherford (2002) and Couch

(2003) are, however, consistently lower than those obtained here (with exception of two short duration experiments of Couch 2003). However, the results of Hammer and Rutherford (2002) and Couch (2003) fall within the uncertainty of our growth rates calculated without taking the nucleation delay into consideration. This further strengthens the importance of accurately estimating nucleation delays when trying to obtain and compare growth rates.

Conclusions

Theoretical (Classical Nucleation Theory) and experimental nucleation delays for decompression-induced crystallization of feldspar in rhyolitic melt agree within a factor of two. This finding opens up the possibility of quantitatively predicting feldspar nucleation during decompression in water-saturated rhyolite. This, thus, provides an opportunity to better understand the timescales of ascent, decompression and nucleation. As part of this, nucleation delay is particularly important to consider for accurate growth rate estimation, particularly under disequilibrium conditions resulting in rapid growth. Nucleation delay can be used to calculate the maximum ascent rate of microlite-free rhyolites and the minimum ascent rate of microlite-bearing rhyolites. We thus extend the simple model for cooling-induced and decompression-induced crystallization, allowing the nucleation delay of felspar in rhyolites to be estimated under a range of eruptive conditions in shallow volcanic systems.

Acknowledgements

This work was supported by a grant overseen by the French National Research Agency (ANR) as part of the "Investissements d'Avenir" Programme LabEx VOLTAIRE (LABX-100-01) and EquipEx PLANEX (ANR-11-EQPX-0036). We extend our gratitude to Rémi Champallier and Ida Di Carlo for assistance with the experimental and analytical techniques, respectively. We would also like to thank Francisco Cáceres and an anonymous reviewer for their comments which helped improve this manuscript and Ulrich Kueppers and Andrew Harris for editorial handling of the manuscript. M.K.R is grateful to Don R. Baker and Shane M. Rooyakkers for helpful discussions.

References:

1. Andrews, B. J., Befus, K. S., 2020. Supersaturation nucleation and growth of plagioclase: a numerical model of decompression induced crystallization. Contributions to Mineralogy and Petrology, 175, 1-20. https://doi.org/10.1007/s00410-020-1660-9
2. Arzilli, F., Carroll, M. R. (2013). Crystallisation kinetics of alkali feldspars in cooling and decompression-induced crystallisation experiments in trachytic melt. Contributions to Mineralogy and Petrology, 166, 1011–1027. doi: 10.1007/s00410-013-0906-1
3. Arzilli, F., Stabile, P., Fabbrizio, A., Landi, P., Scaillet, B., Paris, E., Carroll, M. R. (2020). Crystallisation kinetics of alkali feldspar in peralkaline rhyolitic melts: implications for Pantelleria volcano. Frontiers in Earth Science, 8, 177. doi: 10.3389/feart.2020.00177
4. Baker, D. R. (1990). Chemical interdiffusion of dacite and rhyolite: anhydrous measurements at 1 atm and 10 kbar, application of transition state theory, and diffusion in zoned magma chambers. Contributions to mineralogy and petrology, 104, 407-423. https://doi.org/10.1007/BF01575619
5. Baker, D. R. (1992). Estimation of diffusion coefficients during interdiffusion of geologic melts: application of transition state theory. Chemical Geology, 98, 11-21. https://doi.org/10.1016/0009-2541(92)90089-N
6. Baker, D. R., Rusiecka, M. K., Bilodeau, M., Kwon, S. Y. (2020). Nucleation delay in the anorthite-diopside binary system: Models and experiments. Journal of Non-Crystalline Solids, 546, 120255. https://doi.org/10.1016/j.jnoncrysol.2020.120255
7. Bain, A.A., Kendrick, J.E., Lamur, A., Lavallée, Y., Calder, E.S., Cortés, J.A., Cortés, G.P., Gómez Martinez, D., Torres, R.A. (2021). Micro-textural control on magma rheology and vulcanian explosion cyclicity. Frontiers in Earth Science, 8:611320. https://doi.org/10.3389/feart.2020.611320

8. Becker, R. and Döring, W. (1935). Kinetische Behandlung der Keimbildung in übersättigten Dämpfen. Annales of Physics, 416, 719–752.
9. Blundy, J. D., Cashman, K., Humphreys, M. C. S. (2006). Magma heating by decompression-driven crystallization beneath andesite volcanoes. Nature, 443(7107), 76-80. https://doi.org/10.1038/nature05100
10. Brugger, C. R., Hammer, J. E. (2010). Crystallization kinetics in continuous decompression experiments: implications for interpreting natural magma ascent processes. Journal of Petrology, 51, 1941–1965.
11. Cassidy, M., Manga, M., Cashman, K., Bachmann, O. (2018). Controls on explosive□effusive volcanic eruption styles. Nature Communications, 9, 2839.
12. Castro, J.A., Gardner, J.E. (2008). Did magma ascent rate control the explosive-effusive transition at the Inyo volcanic chain, California? Geology, 36, 279-282. https://doi.org/10.1130/G24453A.1
13. Castro, J.A., Dingwell, D. B. (2009). Rapid ascent of rhyolitic magma at Chaitén volcano, Chile. Nature 461, 780–783. https://doi.org/10.1038/nature08458
14. Couch, S. (2003). Experimental investigation of crystallization kinetics in a haplogranite system. American Mineralogist, 88, 1471–1485.
15. Couch, S., Sparks, R.S.J., Carroll, M.R. (2001). Mineral disequilibrium in lavas explained by convective self-mixing in open magma chambers. Nature 411, 1037–1039. https://doi.org/10.1038/35082540
16. Crameri, F. (2018). Scientific colour-maps. Zenodo. https://doi.org/10.5281/zenodo.1243862
17. Crameri, F., Shephard, G. E., Heron, P. J. (2020). The misuse of colour in science communication. Nature Communications, 11, 5444. https://doi.org/10.1038/s41467-020-19160-7

18. deGraffenried, R. L., Larsen, J. F., Graham, N. A., Cashman, K. V. (2019). The influence of phenocrysts on degassing in crystal□bearing magmas with rhyolitic groundmass melts. Geophysical Research Letters, 46, 5127– 5136.
19. De Yoreo, J. J., Vekilov, P. G. (2003). Principles of crystal nucleation and growth. Reviews in mineralogy and geochemistry, 54, 57-93.
20. Dingwell, D.B. (1996). Volcanic dilemma: Flow or blow? Science, 273, 1054-1055. DOI: 10.1126/science.273.5278.1054
21. D'Oriano, C., Poggianti, E., Bertagnini, A., Cioni, R., Landi, P., Polacci, M., Rosi, M. (2005). Changes in eruptive style during the A.D. 1538 Monte Nuovo eruption (Phlegrean Fields, Italy): the role of syn-eruptive crystallization. Bulletin of Volcanology, 67, 601-621.
22. Eyring, H. (1935). The activated complex in chemical reactions. The journal of chemical physics, 3, 107. https://doi.org/10.1063/1.1749604
23. Fenn, P.M. (1977) The nucleation and growth of alkali feldspars from hydrous melts, Canadian Mineralogist 15, 135-161.
24. Fokin, V. M., Zanotto, E. D., Yuritsyn, N. S., Schmelzer, J. W. (2006). Homogeneous crystal nucleation in silicate glasses: a 40 years perspective. Journal of Non-Crystalline Solids, 352(26), 2681-2714.
25. Gardner, J. E., Denis, M. H. (2004). Heterogeneous bubble nucleation on Fe-Ti oxide crystals in high-silica rhyolitic melts. Geochimica et Cosmochimica Acta, 68(17), 3587-3597. https://doi.org/10.1016/j.gca.2004.02.021
26. Gibbs, J.W. (1875–1878). On the Equilibrium of Heterogeneous Substances. Transactions of the Connecticut Academy of Arts Sciences, 108, 343.
27. Giordano, D., Russell, J. K., Dingwell, D. B. (2008). Viscosity of magmatic liquids: a model. Earth and Planetary Science Letters, 271(1-4), 123-134.

28. Ghiorso, M. S., Sack, R. O. (1995). Chemical Mass Transfer in Magmatic Processes. IV. A Revised and Internally Consistent Thermodynamic Model for the Interpolation and Extrapolation of Liquid-Solid Equilibria in Magmatic Systems at Elevated Temperatures and Pressures. Contributions to Mineralogy and Petrology, 119, 197-212.
29. Ghiorso, M. S., Gualda, G. A. R. (2015). An H_2O–CO_2 mixed fluid saturation model compatible with rhyolite-MELTS. Contributions to Mineralogy and Petrology, 169(6), 1-30. https://doi.org/10.1007/s00410-015-1141-8
30. Glazner, A. F. (2019). The ascent of water-rich magma and decompression heating: A thermodynamic analysis. American Mineralogist: Journal of Earth and Planetary Materials, 104(6), 890-896. https://doi.org/10.2138/am-2019-6925
31. González-García, D., Behrens, H., Petrelli, M., Vetere, F., Morgavi, D., Zhang, C., Perugini, D. (2017). Water-enhanced interdiffusion of major elements between natural shoshonite and high-K rhyolite melts. Chemical Geology, 466, 86-101. https://doi.org/10.1016/j.chemgeo.2017.05.023
32. Gualda G.A.R., Ghiorso M.S., Lemons R.V., Carley T.L. (2012). Rhyolite-MELTS: A modified calibration of MELTS optimized for silica-rich, fluid-bearing magmatic systems. Journal of Petrology, 53, 875-890.
33. Gutzov, I., Schmelzer, J. W. P. (1995). The vitreous state: thermodynamics, structure, rheology, and crystallization. Springer.
34. Hammer, J. E. (2004). Crystal nucleation in hydrous rhyolite: Experimental data applied to classical theory. American Mineralogist, 89, 1673–1679.
35. Hammer, J. E., Cashman, K. V., Hoblitt, R. P., & Newman, S. (1999). Degassing and microlite crystallization during pre-climactic events of the 1991 eruption of Mt. Pinatubo, Philippines. Bulletin of Volcanology, 60(5), 355-380. https://doi.org/10.1007/s004450050238

36. Hammer, J.E. and Rutherford, M. (2002). An experimental study of the kinetics of decompression-induced crystallization in silicic melt. Journal of Geophysical Research, 107, 1-23.
37. Holness, M. B. (2006). Melt–solid dihedral angles of common minerals in natural rocks. Journal of Petrology, 47(4), 791-800. https://doi.org/10.1093/petrology/egi094
38. Huggins, E.G., Ruprecht, R., Ghiorso, M.S. (2021). Using Chemical Affinities to Understand Disequilibrium Textures of Plagioclase Preserved in Magmatic Systems. Geophysical Research Letters, 48 (10), e2021GL092884. https://doi.org/10.1029/2021GL092884
39. Hurwitz, S., Navon, O. (1994). Bubble nucleation in rhyolitic melts: Experiments at high pressure, temperature, and water content. Earth and Planetary Science Letters, 122(3-4), 267-280. https://doi.org/10.1016/0012-821X(94)90001-9
40. Kashchiev, D. (1969). Solution of the non-steady problem in nucleation kinetics. Surface science, 14, 209-220.
41. Kirkpatrick, R. J. (1981). Kinetics of Crystallization of Igneous Rocks in: Lasaga, A.C., Kirkpatrick, R. J. (Eds.), Kinetics of Geochemical, Reviews in Mineralogy, 8, 321-397.
42. Lindoo, A. N., Larsen, J. F., Cashman, K. V., Dunn, A. L., Neill, O. K. (2016). An experimental study of permeability development as a function of crystal□free melt viscosity. Earth and Planetary Science Letters, 435, 45– 5.
43. Mader, H. M., Llewellin, E. W., Mueller, S. P. (2013). The rheology of two-phase magmas: A review and analysis. Journal of Volcanology and Geothermal Research 257, 135–158.
44. Maneta, V., Baker, D. R. (2014). Exploring the effect of lithium on pegmatitic textures: An experimental study. American Mineralogist, 99(7), 1383-1403. https://doi.org/10.2138/am.2014.4556

459 45. Mastin, L. G. (2002). Insights into volcanic conduit flow from an open□source numerical
460 model. Geochemistry, Geophysics, Geosystems, 3(7), 1-18.
461 https://doi.org/10.1029/2001GC000192
462 46. Martel, C. (2012). Eruption dynamics inferred from microlite crystallization experiments:
463 application to Plinian and dome-forming eruptions of Mt. Pelée (Martinique, Lesser
464 Antilles). Journal of Petrology, 53(4), 699-725. https://doi.org/10.1093/petrology/egr076
465 47. Mollard, E., Martel, C., Bourdier, J-L. (2012). Decompression-induced Crystallization in
466 Hydrated Silica-rich Melts: Empirical Models of Experimental Plagioclase Nucleation and
467 Growth Kinetics, Journal of Petrology, 53, 8, 1743–
468 1766, https://doi.org/10.1093/petrology/egs031
469 48. Mollard, E., Martel, C., Le Trong, E., Rogerie, G. (2020). Theoretical models of
470 decompression-induced plagioclase nucleation and growth in hydrated silica-rich
471 melts. Frontiers in Earth Science, 8, 203.
472 49. Moschini, P., Mollo, S., Gaeta, M., Fanara, S., Nazzari, M., Petrone, C. M., Scarlato, P. (2021).
473 Parameterization of clinopyroxene growth kinetics via crystal size distribution (CSD) analysis:
474 Insights into the temporal scales of magma dynamics at Mt. Etna volcano. Lithos, 396, 106225.
475 https://doi.org/10.1016/j.lithos.2021.106225
476 50. Mujin, M., Nakamura, M. (2014). A nanolite record of eruption style transition. Geology, 42,
477 611-614. https://doi.org/10.1130/G35553.1
478 51. Mungall, J. E. (2002). Empirical models relating viscosity and tracer diffusion in magmatic
479 silicate melts. Geochimica et Cosmochimica Acta, 66(1), 125-143.
480 https://doi.org/10.1016/S0016-7037(01)00736-0
481 52. Noguchi, S., Toramaru, A., Shimano, T. (2006). Crystallization of microlites and degassing
482 during magma ascent: Constraints on the fluid mechanical behaviour of magma during the

Tenjo eruption on Kozu island, Japan. Bulletin of Volcanology 68, 432-449. https://doi.org/10.1007/s00445-005-0019-4

53. Pleše, P., Higgins, M. D., Mancini, L., Lanzafame, G., Brun, F., Fife, J. L., Casselman, J., Baker, D. R. (2018). Dynamic observations of vesiculation reveal the role of silicate crystals in bubble nucleation and growth in andesitic magmas. Lithos, 296, 532-546. https://doi.org/10.1016/j.lithos.2017.11.024

54. Polacci, M., Baker, D.R., Mancini, L., Tromba, G., Zanini, F. (2006). Three dimensional investigation of volcanic textures by X-ray microtomography and implications for conduit processes. Geophysical Research Letters 33: L13312. https://doi.org/10.1029/2006GL026241

55. Polacci, M., Arzilli, F., La Spina, G., Le Gall, N., Cai, B., Hartley, M. E. Di Genova, D., Vo, N. T., Nonni, S., Atwood, R. C., Llewellin, E. W., Lee, P. D., Burton, M. R. (2018). Crystallisation in basaltic magmas revealed via in situ 4D synchrotron X-ray microtomography. Scientific Reports 8, 8377.

56. Popa, RG., Bachmann, O., Huber, C. (2021). Explosive or effusive style of volcanic eruption determined by magma storage conditions. Nature Geoscience, 14, 781–786. https://doi.org/10.1038/s41561-021-00827-9

57. Riker, J.M., Cashman, K.V., Rust, A.C., Blundy, J.D. (2015). Experimental constraints on Plagioclase crystallization during H_2O- and H_2O-CO_2- saturated magma decompression. Journal of Petrology 56, 1967-1998.

58. Robie, R. A., Bethke P. M. (1962). Molar volumes and densities of minerals. In: Trace elements investigations, USGS Publication Warehouse, 39 pp. https://doi.org/10.3133/70159012

59. Rusiecka, M. K., Bilodeau, M., Baker, D. R. (2020). Quantification of nucleation delay in magmatic systems: experimental and theoretical approach. Contributions to Mineralogy and Petrology, 175, 47. DOI: https://doi.org/10.1007/s00410-020-01682-4

60. Rusiecka, M.K., Baker, D.R. (2021). Growth and textural evolution during crystallization of quartz and feldspar in hydrous, rhyolitic melt. Contributions to Mineralogy and Petrology, 176, 48. https://doi.org/10.1007/s00410-021-01809-1

61. Rutherford, M. J. (2008). Magma ascent rates. Reviews in Mineralogy and Geochemistry, 69(1), 241-271. https://doi.org/10.2138/rmg.2008.69.7

62. Schmelzer, J. W. P. (2008). Crystal nucleation and growth in glass-forming melts: Experiment and theory. Journal of Non-Crystalline Solids, 354, 269-278.

63. Shannon, R. D. (1976). Revised effective ionic radii and systematic studies of interatomic distances in halides and chalcogenides. Acta Crystallographica, A32, 751-767. https://doi.org/10.1107/S0567739476001551

64. Sharp, T. G., Stevenson, R. J., & Dingwell, D. B. (1996). Microlites and" nanolites" in rhyolitic glass: microstructural and chemical characterization. Bulletin of volcanology, 57(8), 631-640. https://doi.org/10.1007/s004450050116

65. Shea, T. (2017). Bubble nucleation in magmas: a dominantly heterogeneous process?. Journal of Volcanology and Geothermal Research, 343, 155-170. https://doi.org/10.1016/j.jvolgeores.2017.06.025

66. Sirbescu, M. C., Schmidt, C., Veksler, I. V., Whittington, A. G., Wilke, M. (2017). Experimental crystallization of undercooled felsic liquids: generation of pegmatitic texture. Journal of Petrology, 58, 539-568.

67. Slezov, V. V., Schmelzer, J. W. P. (1999). Kinetics of nucleation–growth processes: the first stages. Nucleation Theory and Applications, 6-81.

68. Swanson, S.E. (1977). Relation of crystal-growth rate to the granitic textures. American Mineralogist, 62, 966-978.

69. Toramaru, A. (1991). Model of nucleation and growth of crystals in cooling magmas. Contributions to mineralogy and petrology, 108, 106-117. https://doi.org/10.1007/BF00307330

70. Turnbull, D., Fisher, J. C. (1949). Rate of nucleation in condensed systems. The Journal of chemical physics, 17, 71-73.

71. Volmer, M., Weber, A.Z. (1926) Nucleus Formation in Supersaturated Systems. Zeitschrift für Physikalische Chemie, 119, 277-301.

72. Vona, A., Di Piazza, A., Nicotra, E., Romano, C., Viccaro, M., Giordano, G. (2017). The complex rheology of megacryst-rich magmas: The case of the mugearitic "cicirara" lavas of Mt. Etna volcano. Chemical Geology, 458, 48–67.

Figure and Table Captions:

Figure 1. BSE (back-scattered electron) images of the experimental run products at a, b) 50 MPa (ΔT_{eff} = -55 °C): glass with skeletal feldspar crystals and magnetite, in b) several melt inclusions can be observed; c) 75 MPa (ΔT_{eff} = -20 °C) – glass with feldspar and magnetite crystals and visible vesicle; d) 90 MPa (ΔT_{eff} = -10 °C) well faceted feldspar crystals in glass with magnetite e) low magnification BSE image showing one of the glass chips recovered after the experiment

Figure 2. Nucleation delay of plagioclase in metaluminous rhyolite, empty symbols – no crystals observed, filled symbols – crystals observed, circles – this study, squares – Mollard et al. 2012, solid black curve – nucleation delay calculated using Eq. 1. dotted and dashed lines – nucleation delay curves calculated using the rage of interfacial free energy of 0.10 to 0.25 J/m^2. Pressure relates to this study, while ΔT_{eff} relates to both this study and the study of Mollard et al. 2012.

Figure 3. Growth rates calculated using Eq. 3 at various experimental conditions for average of 10 largest crystals for each samples, circles – this study, squares – Couch 2003, stars – Hammer and Rutherford 2002; Pressure relates to this study, while ΔT_{eff} is relevant for all the presented studies.

554 **Figure 4.** Growth rates calculated using Eq. 3 at 50 MPa at various experimental durations (48, 72 and
555 120 h) for average of 10 largest crystals for each sample, black symbols – growth rates calculated with
556 taking nucleation delay into consideration, grey symbols – growth rates calculated without taking
557 nucleation delay into consideration, dashed line – exponential trend line fitted to the data.
558 **Figure 5.** Nucleation delay curves for homogeneous (solid black curve) and heterogeneous (dotted black
559 curved) nucleation of feldspar calculated using the theoretical model for feldspar nucleation in water-
560 saturated rhyolite, grey dashed lines – ascent paths.
561 **Figure 6.** Nucleation delay calculated in the PT space for water-saturated rhyolite with the model and
562 parameters described in the text of the manuscript. Colormap 'hawaii' (Crameri 2018, Crameri et al.
563 2020) was used to ensure accessibility for readers.
564 **Table 1.** Experimental run table, LCOL – experiments conducted to confirm the location of the liquidus
565 calculated using MELTS, LCOD – decompression single step decompression (SSD) experiments; P_i –
566 initial pressure, P_f – final pressure, ΔT_{eff} – effective undercooling, dP/t – rate of decompression, gl –
567 glass, mgt – magnetite, fds – feldspar.

Figure 1a

Click here to access/download;Figure;Figure1a.tif

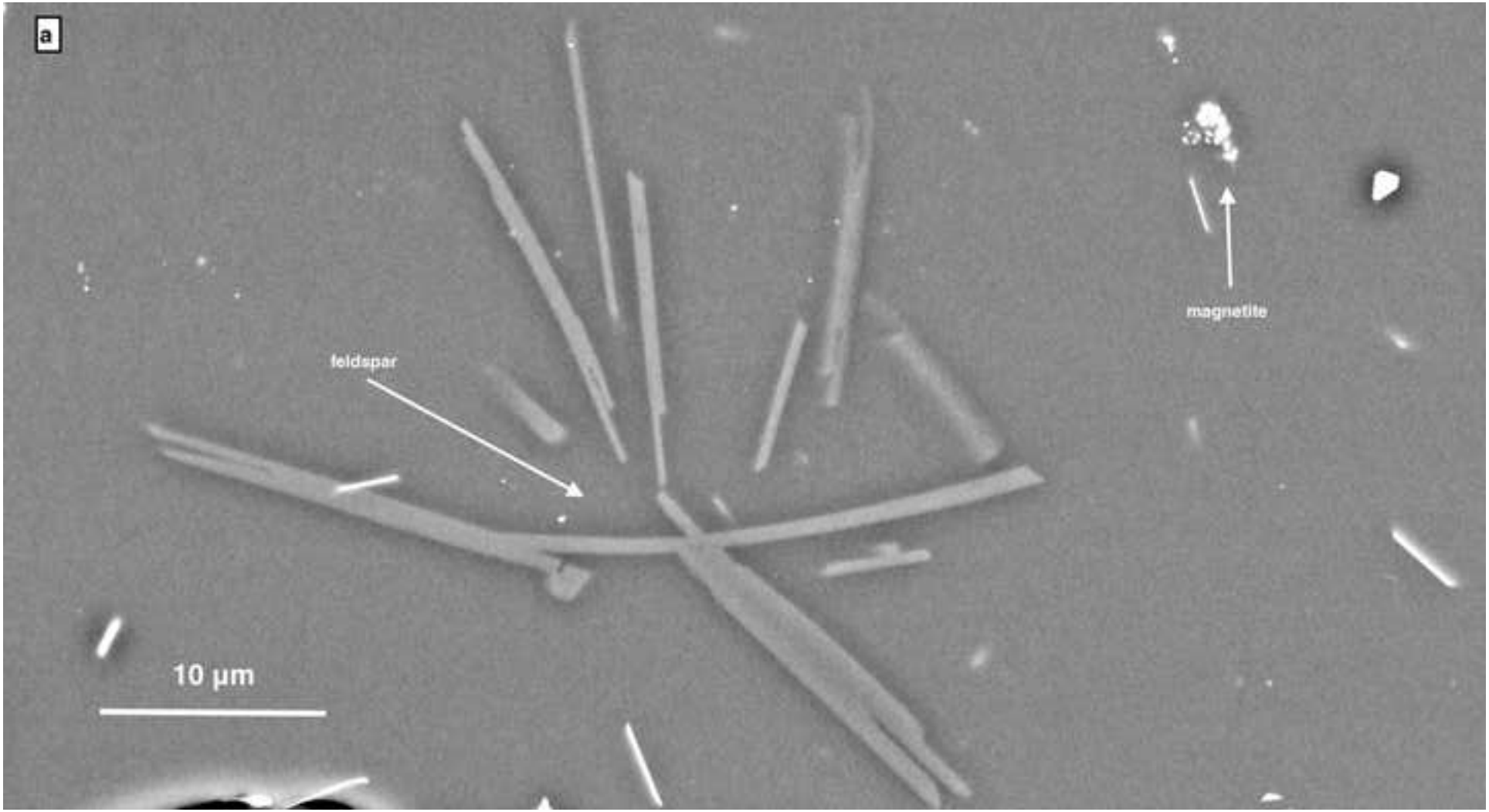

Figure 1b

Click here to access/download;Figure;Figure1b.tif

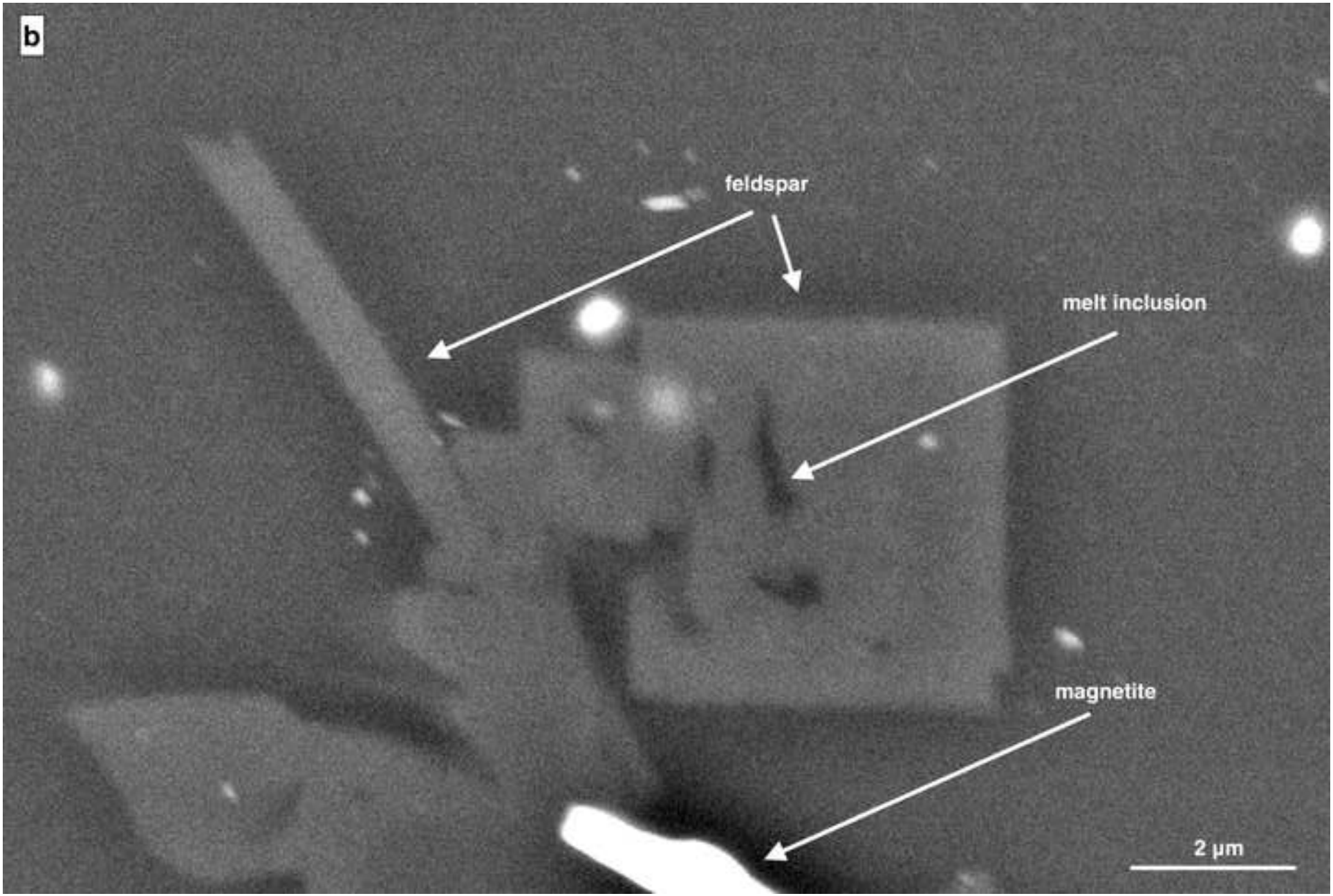

Figure 1c

Click here to access/download;Figure;Figure1c.tif

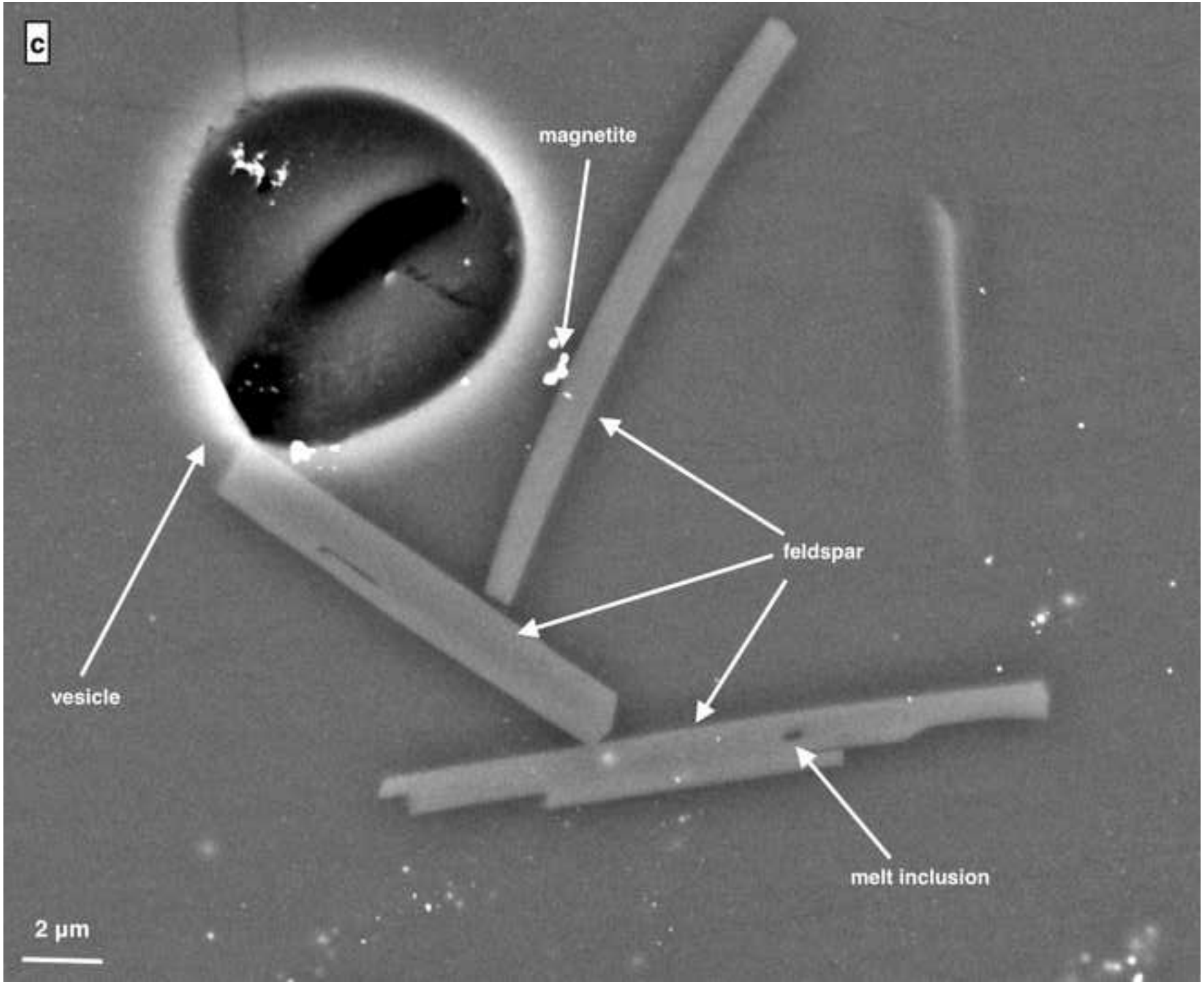

Figure 1d

Click here to access/download;Figure;Figure1d.tif

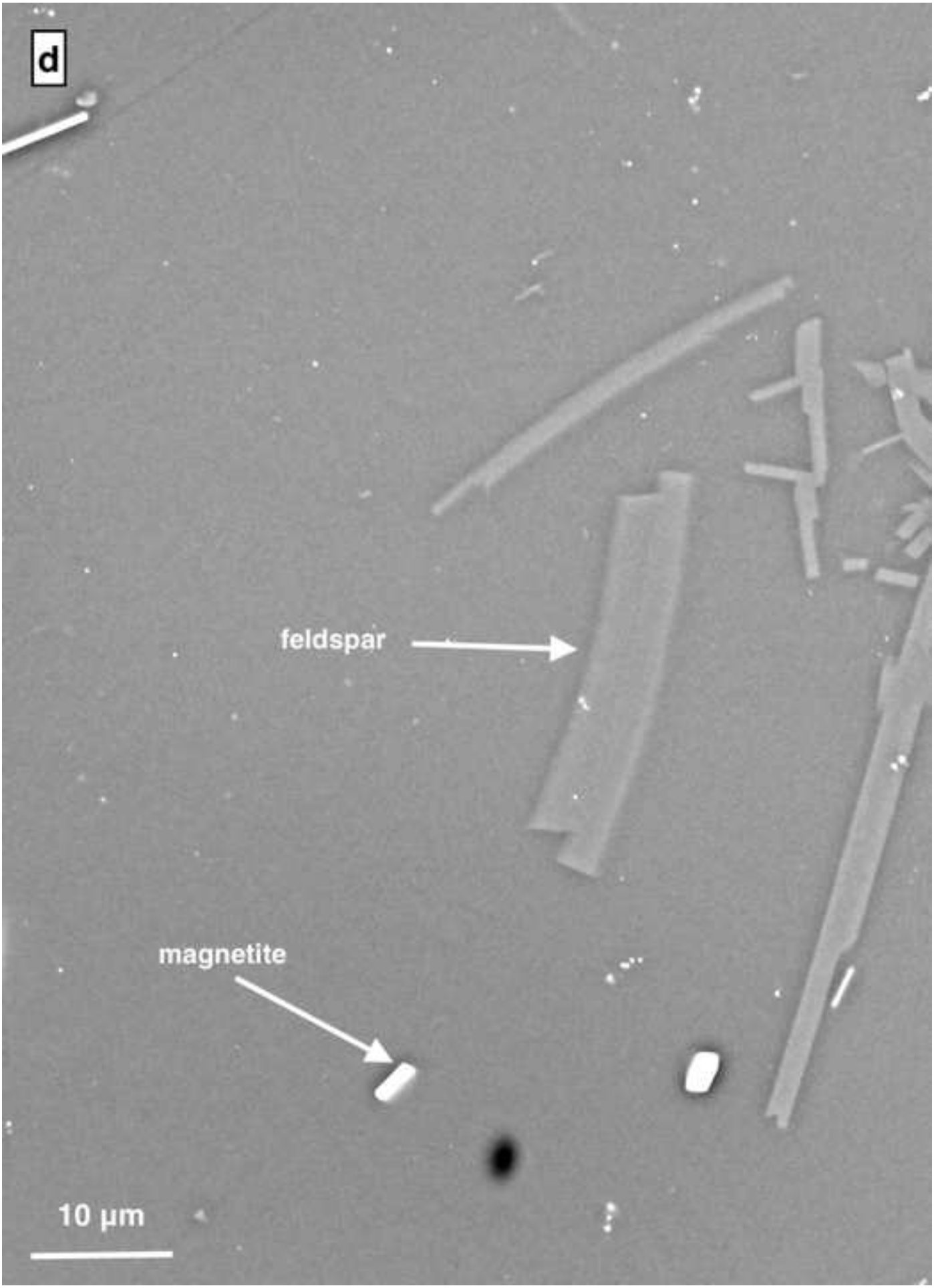

Figure 1e

Click here to access/download;Figure;Figure1e.tif

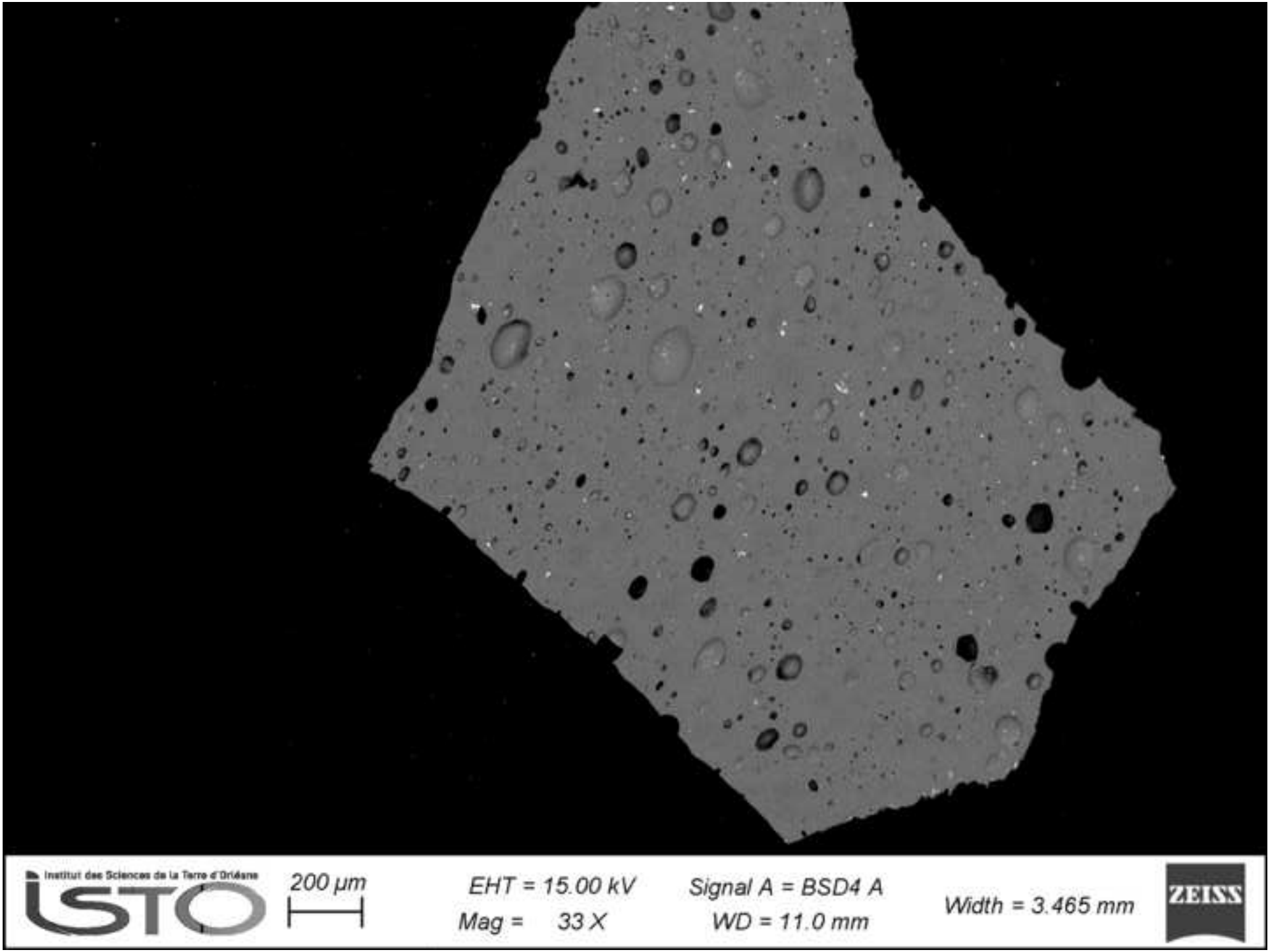

Figure 2

Click here to access/download;Figure;Figure2revised.tif

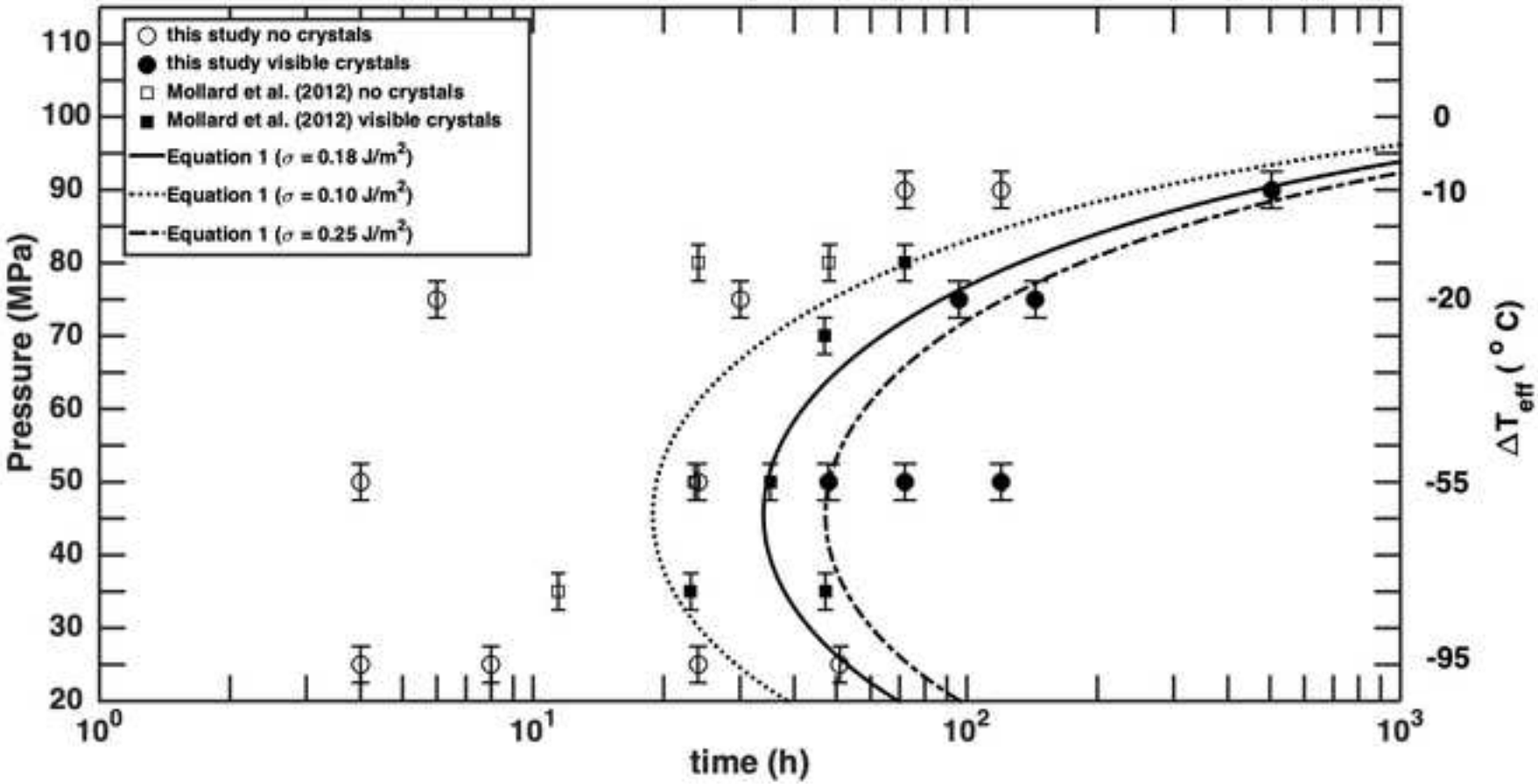

Figure 3

Click here to access/download;Figure;Figure3revised.tif

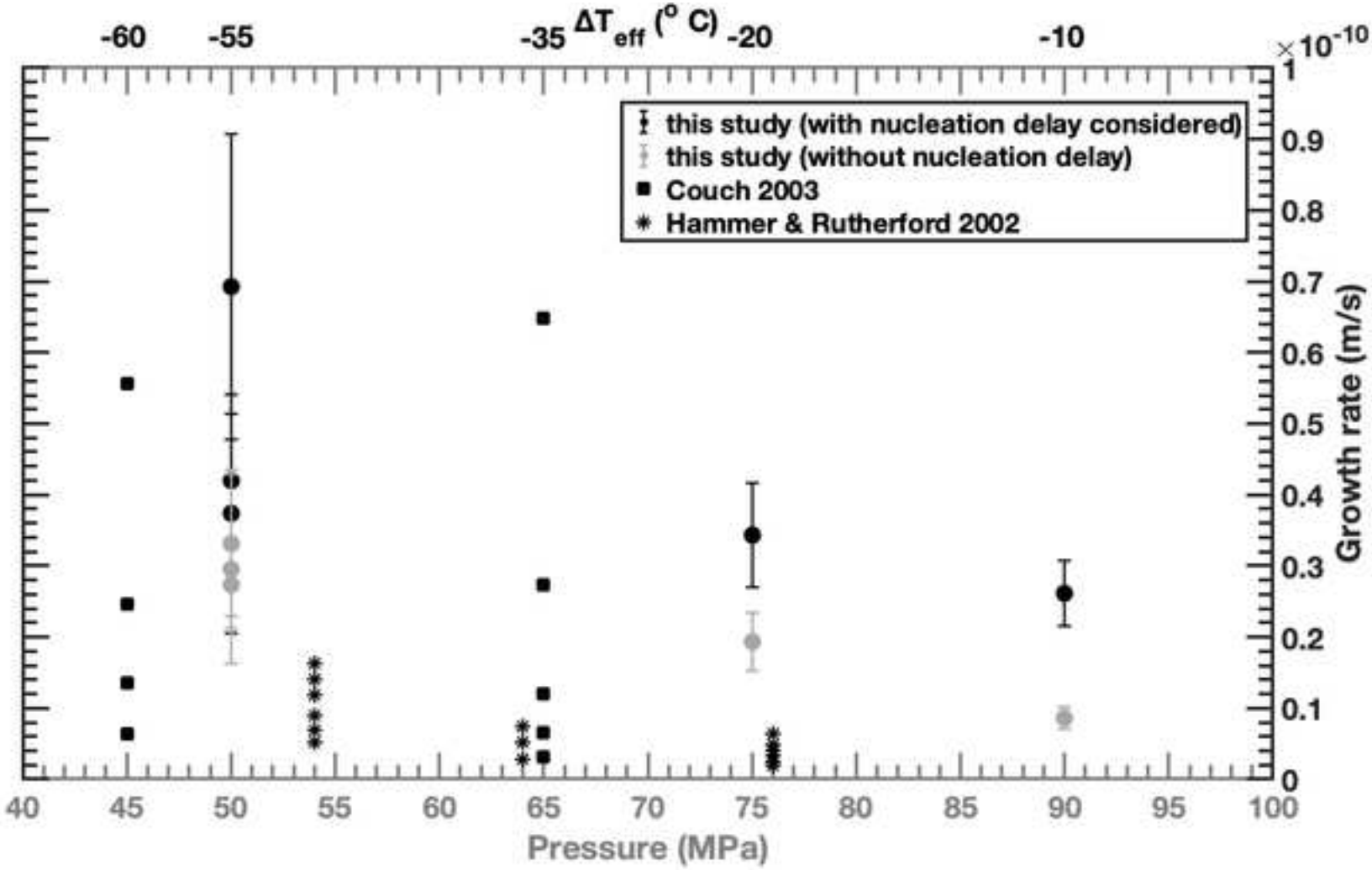

Figure 4

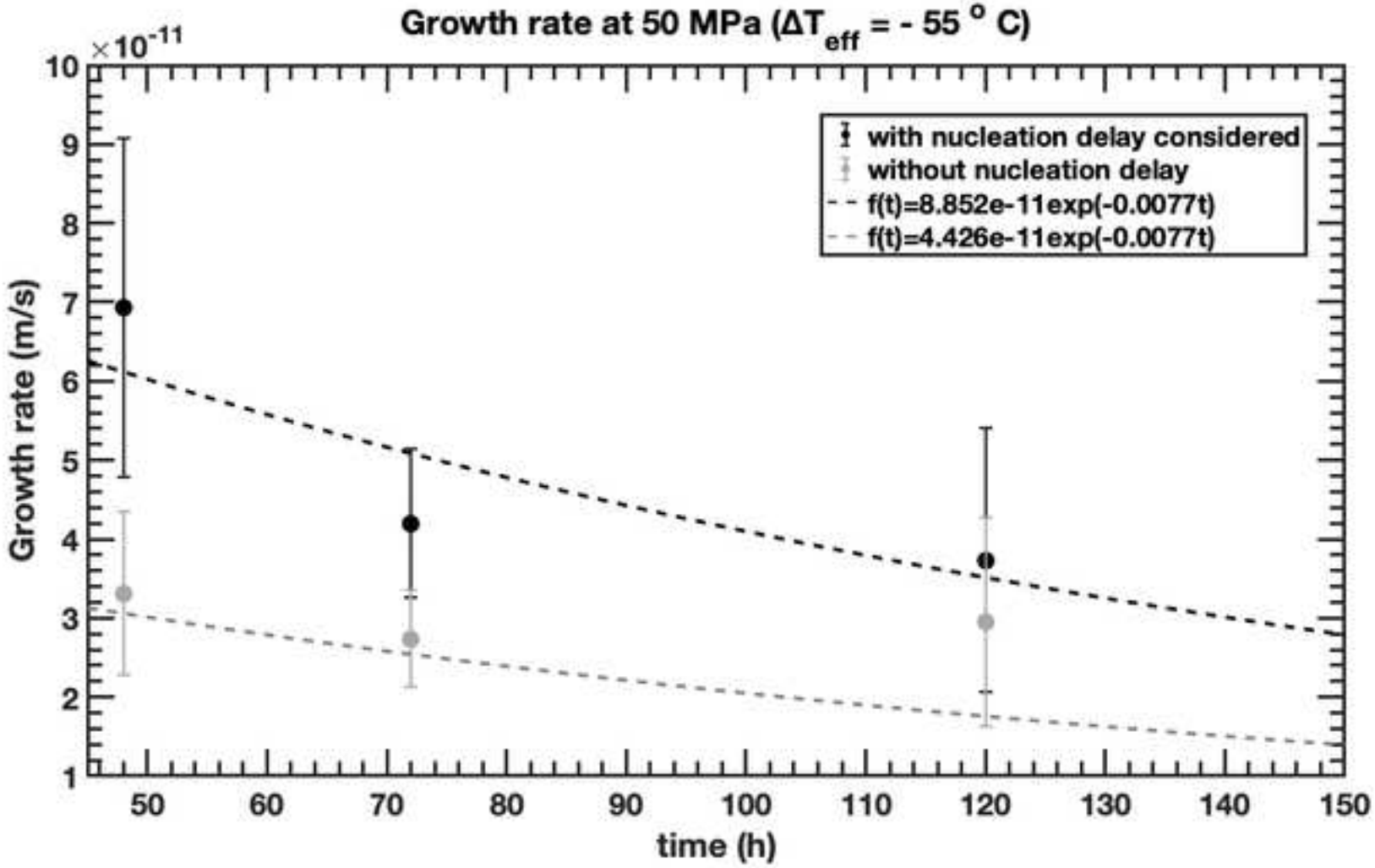

Figure 5

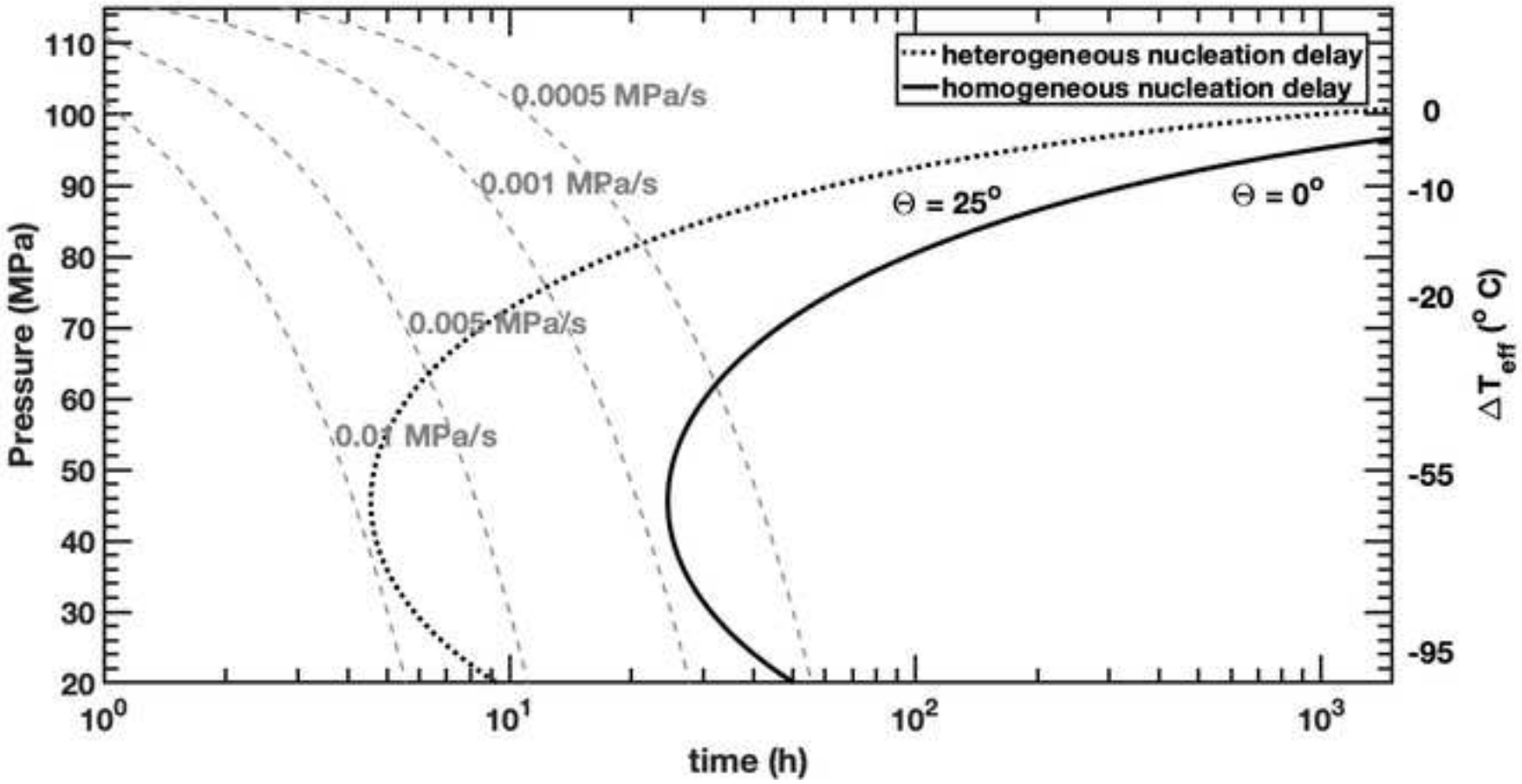

Figure 6

Click here to access/download;Figure;Figure6revised.tif

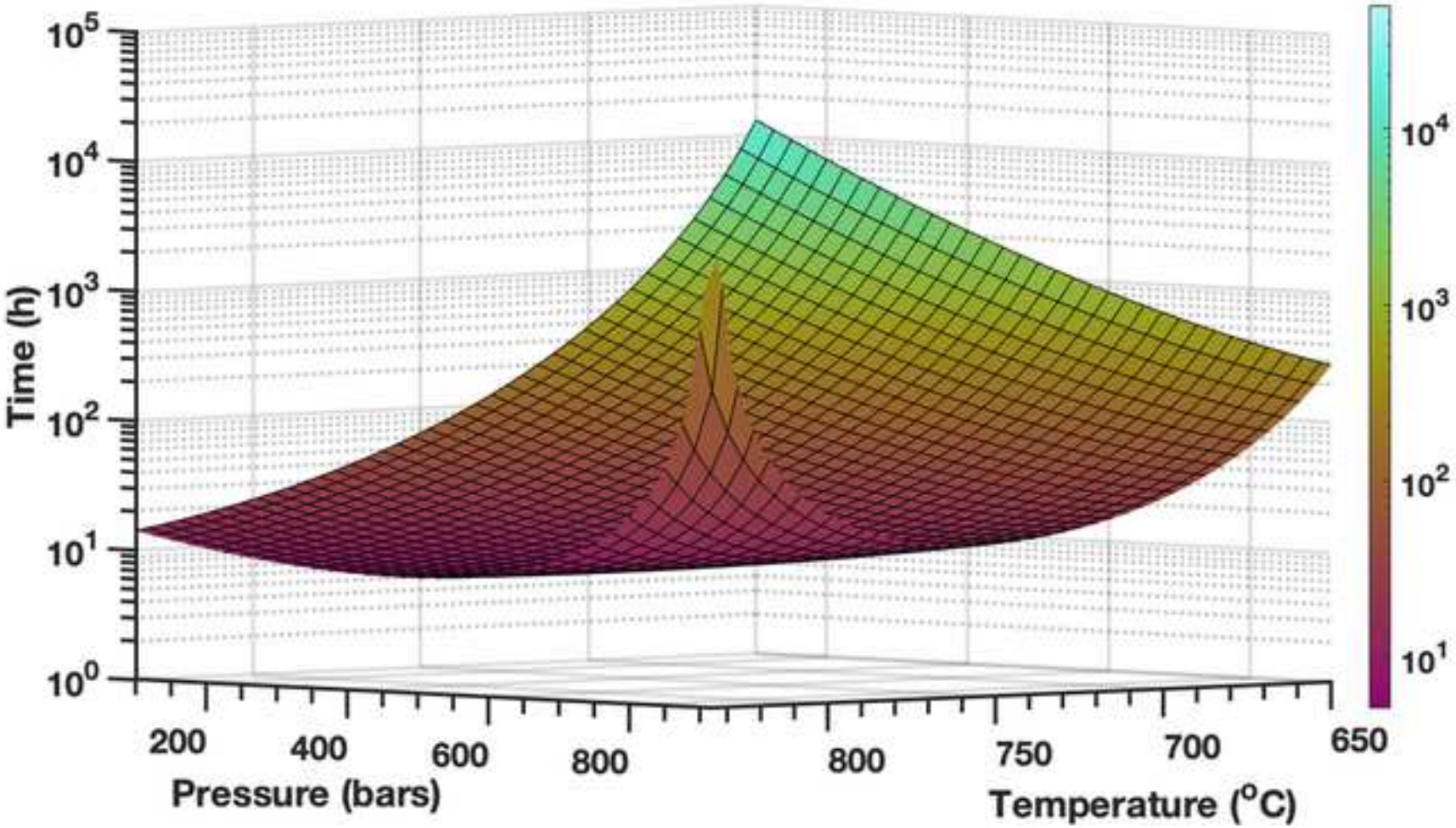

Table 1

Sheet1

sample	T (°C)	P_i (MPa)	P_f (MPa)	dP/t (MPa/h)	ΔT_{eff} (°C)	time at P_f (h)
LCOD-50	825	200	50	600	-55	0
LCOD-25-4	825	200	25	600	-95	4
LCOD-25-8	825	200	25	600	-95	8
LCOD-25-24	825	200	25	600	-95	24
LCOD-25-51	825	200	25	600	-95	51
LCOD-50-4	825	200	50	600	-55	4
LCOD50-24	825	200	50	600	-55	24
LCOD-50-48	825	200	50	600	-55	48
LCOD-50-72	825	200	50	600	-55	72
LCOD-50-120	825	200	50	600	-55	120
LCOD-75-6	825	200	75	600	-20	6
LCOD-75-30	825	200	75	600	-20	30
LCOD-75-96	825	200	75	600	-20	96
LCOD-75-144	825	200	75	600	-20	144
LCOD-90-72	825	200	90	600	-10	72
LCOD-90-120	825	200	90	600	-10	120
LCOD-90-504	825	200	90	600	-10	504
LCOL200	800	200	200	-	-	168
LCOL200	825	200	200	-	-	168
LCOL200	850	200	200	-	-	168
LCOL200	900	200	200	-	-	168
LCOL150	825	200	200	-	-	168
LCOL50	850	200	200	-	-	168
LCOL50	900	200	200	-	-	168

* phases: gl – glass; mgt – magnetite; fds – feldspar;

nucleation	phases
no	gl+mgt
no	gl+mgt
no	gl+mgt
no	gl+mgt
no	gl+mgt
no	gl+mgt
no	gl+mgt
yes	gl+mgt+fds
yes	gl+mgt+fds
yes	gl+mgt+fds
no	gl+mgt
no	gl+mgt
yes	gl+mgt+fds
yes	gl+mgt+fds
no	gl+mgt
no	gl+mgt
yes	gl+mgt+fds
-	gl+mgt+fds
-	gl+mgt
-	gl+mgt
-	gl+mgt
-	gl+mgt
-	gl+mgt+fds
-	gl+mgt